PAPER • OPEN ACCESS

ITO-free OLEDs utilizing inkjet-printed and low temperature plasma-sintered Ag electrodes

View the article online for updates and enhancements.

Flexible and Printed Electronics

PAPER

ITO-free OLEDs utilizing inkjet-printed and low temperature plasma-sintered Ag electrodes

Michael Hengge[1] , Konstantin Livanov[2] , Natalia Zamoshchik[2] , Felix Hermerschmidt[3]
and Emil J W List-Kratochvil[1,3]

[1] Helmholtz-Zentrum Berlin für Materialien und Energie GmbH, Hahn-Meitner-Platz 1, 14109 Berlin, Germany
[2] OrelTech GmbH, Rudower Chaussee 29, 12489 Berlin, Germany
[3] Institut für Physik, Institut für Chemie & IRIS Adlershof, Humboldt-Universität zu Berlin, Brook-Taylor-Straße 6, 12489 Berlin, Germany

E-mail: felix.hermerschmidt@hu-berlin.de

Abstract

We report an inkjet-printed indium tin oxide (ITO)-free electrode made from a particle-free silver ink. After printing, an argon plasma is used to reduce the silver ions in the ink to metallic silver. This process does not require high temperatures and is therefore suitable for use with temperature sensitive substrates. Printed silver layers show good optical transmittance and electrical conductivity. To demonstrate the capabilities of the electrodes, inverted ITO-free organic light-emitting diodes (OLEDs) were produced via solution processing. In terms of luminance and efficacy, the devices containing the printed electrodes show improved luminance and current efficacy compared to ITO-based reference devices. When fabricated with flexible substrates, the printed OLEDs show high bending stability, enabling flexible applications.

1. Introduction

Many of today's electronic devices are equipped with touch screens incorporating transparent electrodes (TEs). These are mostly made of transparent metal oxides which allow the light to pass through while retaining high electrical conductivity. The same electrodes are used in organic light-emitting diodes (OLEDs). In contrast to LEDs, where the light emitting chip is contacted with at least one bonding wire, OLEDs use planar electrodes which cover the whole active area. Therefore, the generated light has to traverse at least one of the contacts in order to leave the device. With its high optical transmission over the whole visible spectrum and its low sheet resistance, indium tin oxide (ITO) is the de facto standard in most modern applications [1, 2]. Because industrial trends are moving towards flexible devices and large-area production [3], in these applications the high brittleness is one of the biggest drawbacks of ITO and must be taken into account [4].

The search for alternative TEs has led to two main approaches distinguished by their processing method. The first of these is thermal evaporation of thin metallic films [5] or dielectric-metal-dielectric compounds [6], the second are solution-based methods such as screen printing, roll-to-roll printing, spray coating and inkjet printing [7, 8]. As an additive manufacturing technique, inkjet printing benefits from a very small loss in starting material compared to other methods. As a drop-on-demand technique, it is able to directly produce paths on substrates without the need for masks or other pre-patterning of the substrate. Frequently used materials in solution processing are metal nanowires, carbon materials such as graphene or carbon nanotubes [9], metal nanoparticle inks [10], or metal-organic decomposition (MOD) inks [7, 11]. These MOD inks are fabricated by dissolving mostly oxidized metal precursors and additives such as stabilizing agents in suitable solvents or by complexing metal ions with organic ligands [12]. As a result, the inks have a longer shelf-life, since there is no (or greatly reduced) particle agglomeration [13].

When the aforementioned inks are used in electrode production, two different goals can be pursued. Fully TEs with an overall transmission of >80% [9] can be manufactured. In this case nanowire inks made

from metals such as gold [14], silver [15] or copper [16] as well as carbon-based inks (graphene, nanotubes) [9] are the materials of choice. These typically achieve sheet resistances of 10–13 Ω sq^{-1} at 80% transmission for silver [17], 5–20 Ω sq^{-1} at 60%–65% transmission for copper [16] and 50–100 Ω sq^{-1} at 85%–90% transmission for carbon-based layers [18].

The second type of electrode is a non-transparent one, where mostly nanoparticle inks made from silver [19] or copper [20] are used. Given their opaque nature such electrodes cannot cover the whole device area without blocking all the light and are therefore typically applied in thin lines. These lines are interconnected to form linear or hexagonal grids [10]. Such structures exhibit a transmission which is dependent on the grid parameters such as the line width and line spacing, but typical transmission values are >75% while the sheet resistance is in the range of 0.2–20 Ω sq^{-1} [10]. Both, the fully transparent and grid electrodes show a higher resilience to bending stress than ITO [21], with a reported increase in resistance (relative to the initial value) after several hundred bending cycles of only around two times for both nanowires and metal grids [15, 22].

Most solution-based materials require a post treatment process (sintering) to reach their full conductivity. Firstly, the aim of this process is to drive of excess solvent. Protective capping agents, which are added by the ink manufacturer to stabilize the ink, are removed [7]. Secondly, with inks made from metal nanoparticles, the particles can merge into a homogeneous layer [7]. The MOD inks, on the other hand, decompose, meaning the metal precursors are reduced to form a metallic layer [13].

This sintering process can be achieved by a variety of different methods such as thermal sintering [23], photonic sintering [24] (flash or laser sintering), electrical [25], or plasma sintering [12, 26–29]. However, in the case of nanoparticle inks, all the above-mentioned techniques except plasma sintering rely on the transfer of heat to the metal particles. This transfer is either achieved by directly heating the samples (thermal sintering) or the absorption of light (flash, laser sintering) or electrical energy which then is converted to heat inside the ink itself. The heat is used to decompose non-volatile ink ingredients such as stabilizing agents [9, 23]. For the heat-driven processes it is important to consider the thermal conductivity of the ink and the substrate material to obtain an optimal result [30]. When choosing a sintering temperature, care must be taken to avoid damaging the sample from overheating, which can cause cracks or holes in the final film [23]. The sintering temperature of 150 °C or more, required for most inks, makes thermal sintering hard to use on flexible substrates with a lower glass-transition temperature such as PET (T_g = 70 °C–80 °C) [31, 32].

In contrast to that, plasma sintering mostly relies on a low-pressure atmosphere to free the metal particles from undesired compounds [27]. Here the sample is brought into a low-pressure environment which is enough to evaporate most of the organic solvents. Longer chained solvents and other organic compounds are then broken down by the plasma species into shorter, more volatile constituents [33]. However, atmospheric pressure plasma sintering has also been reported with and without added thermal sintering [28, 29]. Another, seldom used, plasma process is the direct reduction of MOD inks via the plasma species [34]. In this case, a reducing gas can be used to enable chemical reduction from an ionized species to elemental metal. Even though the knowledge of this process itself goes back as far as 1887 [35], there are only a few examples of applying this process to partially or fully plasma-assisted metallization of surfaces in recent literature [34, 36–38]. While this method requires a vacuum chamber and the necessary gas connections, higher temperatures are normally not used or generated, which makes the method compatible with temperature-sensitive flexible substrates.

In this work we present electrodes made from a MOD ink that uses argon plasma to reduce the printed layer. A thin, transparent, and highly conductive silver layer is formed. No reducing gas such as H$_2$ is needed. Our production process uses very low temperatures and is therefore also suitable for temperature-sensitive substrate materials.

2. Experimental

OTech T 1053 plasma metallization inks were provided by OrelTech GmbH. The inks consist of a mixture of organic solvents that facilitate ink printing and a metallic precursor that contains Ag$^+$ cations [39]. Viscosity measurements of the ink were performed using an Ostwald (U-tube glass capillary) viscometer. Surface tension was assessed using the drop weight method. This method uses the correlation between the surface tension and the weight of a drop of liquid that has only just detached from a capillary. In combination with the mass and surface tension of a drop of a reference liquid, the unknown surface tension can be calculated [40, 41]. X-ray powder diffraction (XRD) experiments were performed using a Rigaku TTRAX III (18 kW) instrument with K$_\alpha$ radiation of Cu (1.54 Å) and parallel beam configuration. The scanning angle was varied from 15° to 47° with steps of 0.025° in 2θ mode. Silicon was used as a substrate for the XRD measurements as its defined diffraction signature peaks can in most cases be easily recognized and differentiated from the investigated specimen peaks. Glass and PET, on the other hand, are substrates with partially amorphous composition which manifests in XRD as unspecified broad bands and makes the film's peak identification more complicated.

ITO-coated glass samples with a size of 20 × 15 mm and an ITO thickness of 120 nm were purchased from Psiotec Ltd. The samples were thoroughly wiped with acetone and isopropanol and dried with nitrogen before being used.

Glass substrates for printing were cleaned in the same way. The printing was performed on a PiXDRO LP50 inkjet printer (Meyer Burger/Süss Microtec). A Spectra S-Class printhead with a nominal drop volume of 30 pl was used at a resolution of 850 dpi. After printing, the samples were transferred to a Femto plasma system (Diener) where they were vacuum dried until a pressure of lower than 0.1 mbar was reached inside the chamber. When completely dry, an argon plasma with a gas flow of 20 sccm and a power of 250 W was applied for 5 min to reduce the samples to metallic silver. The time this drying takes was found to be dependent on the sample size while the curing time itself was not.

Absorption spectra of the printed silver and the reference ITO were measured with a Perkin Elmer Lambda 950 double beam spectrometer. Surface analysis was performed with a scanning force microscope (SFM) (Bruker FastScan) using the tapping mode and a LEXT OLS4100 confocal laser microscope (Olympus). The resulting images were analyzed using open-source software (Gwyddion). Sheet resistance measurements were carried out with a four-point probe (Jandel).

The haze of the printed layers was assessed qualitatively by looking at the diffusion of laser light through the printed samples. A green laser was shone through the sample at a distance of 1 cm. On a screen at 1 m distance behind the sample, the size of the diffusion pattern was assessed.

When preparing the OLED devices, the sample surface was activated with another 5 min of argon plasma treatment. On top of this a zinc oxide:polyethylene imine (ZnO:PEI) blend (2:1 by volume) was spin coated at 2500 rpm and dried on a hotplate at 120 °C for 10 min leading to a 15 nm thick layer. The ZnO nanoparticle dispersion (Genesink, 12 nm particles, 1% dispersion in isopropanol) was used as received, while the PEI (Sigma Aldrich, with a molecular weight of 25 000 g mol^{-1}) was dissolved in isopropanol at a concentration of 0.4 wt% according to [42]. The PDY-132 (Super Yellow, Sigma-Aldrich) emissive layer was spin coated from a 5 mg ml^{-1} toluene solution at 2500 rpm for 60 s resulting in a thickness of 80 nm. All printing and spin coating steps were performed in ambient conditions. A top electrode consisting of 10 nm MoO_3 and 200 nm Ag was then thermally evaporated in vacuum at a base pressure of 10^{-6} mbar using a shadow mask to yield a device area of 0.49 cm^2. Finally, all devices were encapsulated by putting a drop of UV-curable resin (Ossila) on top of the OLED and adding a glass lid. The resin was then cured under 365 nm light for 10 min.

To prepare flexible devices, PET substrates were cleaned thoroughly with isopropanol. The ITO coated PET samples were purchased from PsioTec Ltd. The same fabrication process as for the glass samples was used with the exception of a lower drying temperature of 100 °C for the ZnO:PEI layer. Encapsulation was done using another layer of PET but with the same UV-curable resin.

Current density–voltage–luminance characterization (JVL) was performed with a Keithley 2612B source meter and a Konica Minolta LS-160 luminance meter in a purpose-built setup. Electroluminescence (EL) spectra were taken with a CS2000 spectrometer (Ocean Optics) using OceanView software.

Bending tests were performed by measurement of the sheet resistance at set intervals of manual bending against a fixed radius. The cyclic strain was calculated according to the details described in the main text.
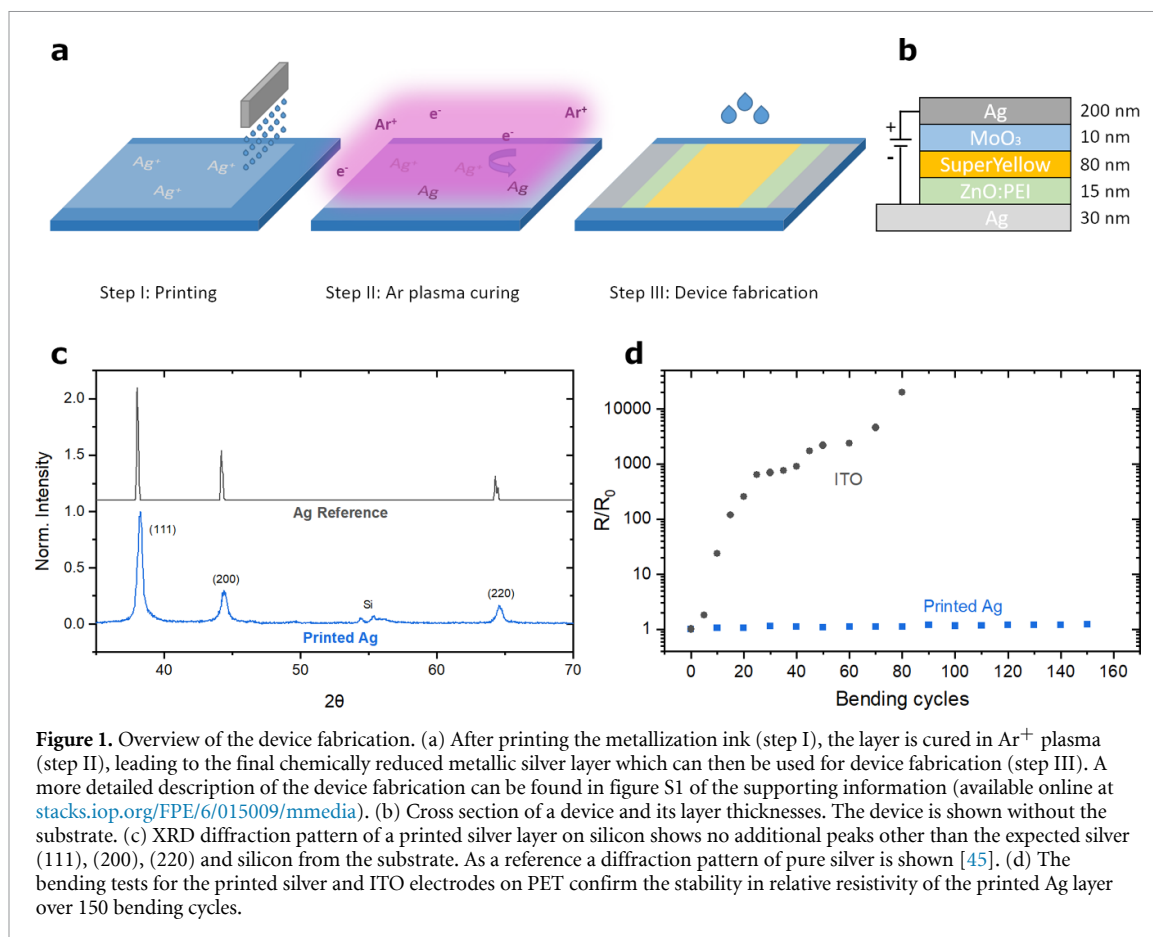
3. Results and discussion

3.1. Ink development and printing

The metallization ink used in this study (OTech T 1053) was optimized for an inkjet printing deposition method. It has a viscosity in the range of 10–12 cP and surface tension in the range of 25–30 mN m^{-1} at room temperature. As the ink is subjected to plasma irradiation, Ag$^+$ ions in the ink undergo a rapid reduction to Ag^0 particles, that accumulate into a metallic silver layer [36]. Reduction of metallic precursors by a similar plasma process has been discussed in literature [38, 43, 44]. The full mechanism of the reaction, however, remains to be thoroughly studied. During the metallization process, the temperature rises only to 40 °C–50 °C, thus making the process safe for most substrates.

The resulting parameters of the printed silver electrode, such as transmission, conductivity, roughness, and others strongly depend on the formulation of the metallization ink, the printing process and plasma conditions. The argon gas flow, plasma power and treatment duration stated in the experimental section were found to be optimal when using the OTech T 1053 ink. The XRD diffractogram of the metallic layers printed with the OTech T 1053 ink is shown in figure 1(c). Since no peaks other than the expected silver (111), (200), (220) ones were found, the plasma metallization process is able to remove all residual organic compounds.

Figure 1(a) shows the production process for the printed silver electrodes. In the first step the electrode structure was printed on the cleaned substrates at a resolution of 850 dpi and a drop volume of 30 pl. Early trials showed a strong so-called coffee-ring effect, which is the flow of ink towards the edge of a drying printed area [46]. This was significantly reduced by a short plasma treatment of the cleaned substrate before printing and carefully optimizing the plasma treatment parameters. Due to the particle-free nature

Figure 1. Overview of the device fabrication. (a) After printing the metallization ink (step I), the layer is cured in Ar^+ plasma (step II), leading to the final chemically reduced metallic silver layer which can then be used for device fabrication (step III). A more detailed description of the device fabrication can be found in figure S1 of the supporting information (available online at stacks.iop.org/FPE/6/015009/mmedia). (b) Cross section of a device and its layer thicknesses. The device is shown without the substrate. (c) XRD diffraction pattern of a printed silver layer on silicon shows no additional peaks other than the expected silver (111), (200), (220) and silicon from the substrate. As a reference a diffraction pattern of pure silver is shown [45]. (d) The bending tests for the printed silver and ITO electrodes on PET confirm the stability in relative resistivity of the printed Ag layer over 150 bending cycles.

of the MOD ink used, clogging of the printhead was not an issue and the same printheads could be used for over half a year.

The samples were then transferred to the plasma chamber. The second step consists of drying the samples in a low-pressure atmosphere with a pressure of under 0.1 mbar. Afterwards, an argon plasma was applied to cure the samples. These layers were then analyzed and compared to commercial ITO electrodes.
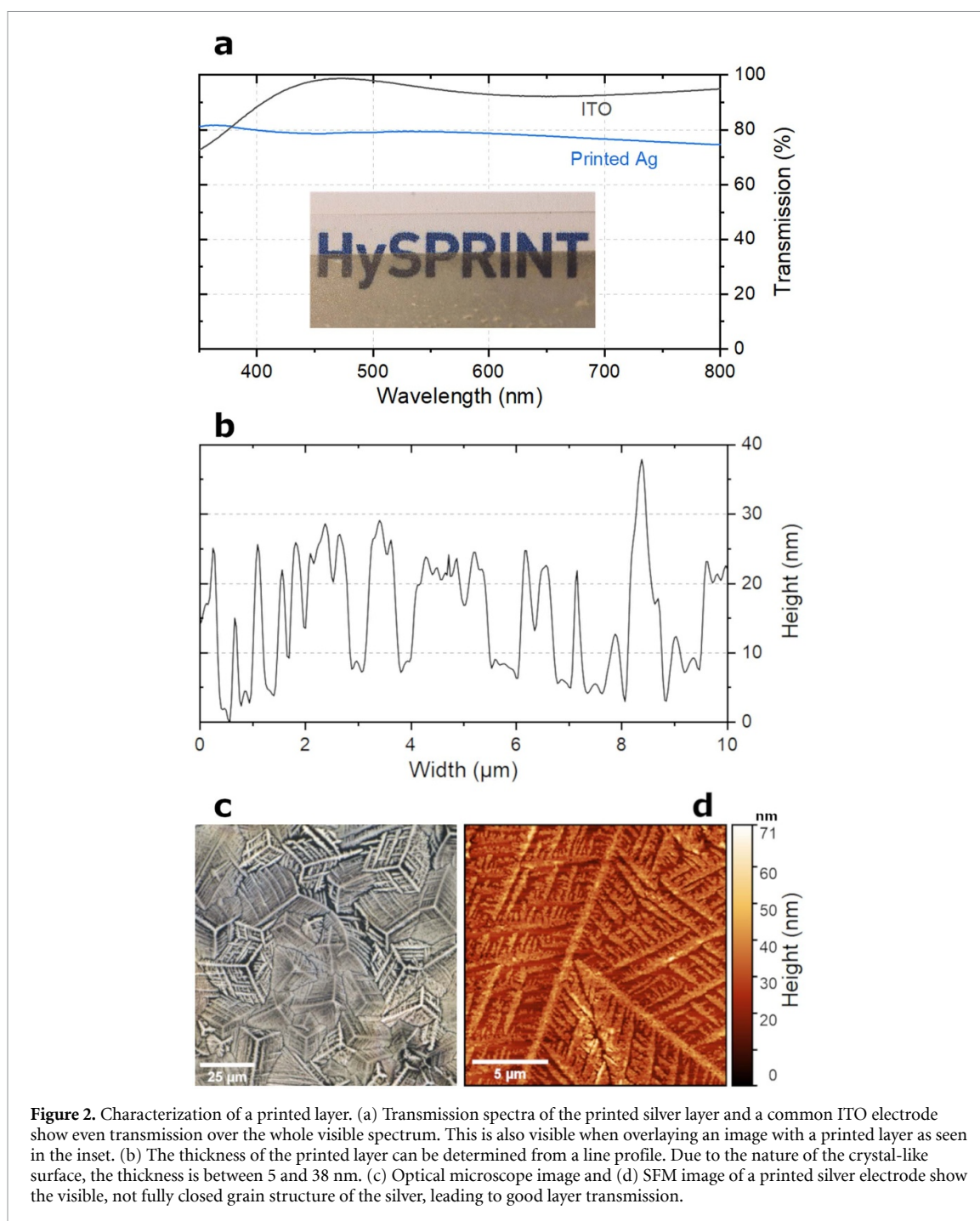
3.2. Printed electrode characterization

Transmission measurements were carried out to compare the two different electrode materials. Figure 2(a) shows the transmission curves of ITO and printed Ag over the visible spectrum measured on glass substrates. Both display a high transmission for visible light. ITO reaches up to 98% transmission while the printed silver layer is able to achieve 75%–80% over the whole visible spectrum. This high transmission enables OLEDs with printed electrodes to have an accurate color representation. However, transmission and conductivity are strongly thickness dependent. While thicker films show enhanced electrical conductivity, the transmission decreases, negating the positive effect on device efficacy.

Our layers, with a thickness of 30 nm (due to the crystalline nature of the printed silver layer, the thickness can be thinner in some places), as can be seen

in figure 2(b), and a sheet resistance of 16 Ω sq^{-1} demonstrate a good compromise of both values and are in good agreement with other recently published results, as shown in the introduction.

One of the reasons for the good optical transmission of the printed silver can be seen in figure 2. When drying, the silver in the ink forms a crystalline structure which is not fully closed, thus allowing light to pass through. This structure is maintained throughout the metallization process. Figure 2(c) shows a fully cured layer in an optical microscope image. Different grain structures can be seen. The more closed features enhance the electrical conductivity. In figure 2(d) an SFM image of a closed section is shown. One can clearly see that the needle like features of the printed layer are present up to a very small scale.

Furthermore, when printed on flexible PET substrates, the transparent silver layers show a high degree of flexibility through 150 manual bending cycles. Using the relation $\varepsilon = d_s/2r$, where d_s is the thickness of the bent sample and r the bending radius, the cyclic strain ε was calculated [47]. While more elaborated and automated testing methods were reported before [47–49], these manual tests already show sufficiently the high flexibility of thin printed silver. The applied bending radius is 5 mm, corresponding to 2% of cyclic strain. As can be seen in figure 1(d), the printed silver layers show next to no degradation in terms of relative resistance R/R_0.

Figure 2. Characterization of a printed layer. (a) Transmission spectra of the printed silver layer and a common ITO electrode show even transmission over the whole visible spectrum. This is also visible when overlaying an image with a printed layer as seen in the inset. (b) The thickness of the printed layer can be determined from a line profile. Due to the nature of the crystal-like surface, the thickness is between 5 and 38 nm. (c) Optical microscope image and (d) SFM image of a printed silver electrode show the visible, not fully closed grain structure of the silver, leading to good layer transmission.

Again, this agrees well with state-of-the-art electrodes as discussed previously. In contrast to that the relative ITO resistance doubles after only five bending cycles. After 15 cycles the relative ITO resistance is over 100 times greater and critical failure (no measurable conductivity) occurs after only 80 bends. Thus, the printed Ag shows excellent performance in terms of flexibility compared to the brittle ITO.

A qualitative haze assessment of the printed film in comparison to ITO is shown in figure S2 of the supporting information. While this measurement does not provide the conclusive results a quantitative full-spectrum haze measurement would produce, it does give a qualitative indication of the electrode properties. Upon shining a green laser through the substrates and analyzing the size of the projected pattern, PET substrates with ITO show a slightly larger laser pattern compared to substrates with printed silver, which correlates to more haze than the printed silver layers on PET.

3.3. Functional device characterization

To characterize the performance of the printed layers in comparison to ITO, bottom-emitting OLEDs with an active area of 0.49 cm^2 were fabricated using both electrode materials on glass and flexible PET substrates. To quantify the electrical properties of the fabricated OLED devices, JVL curves were measured.
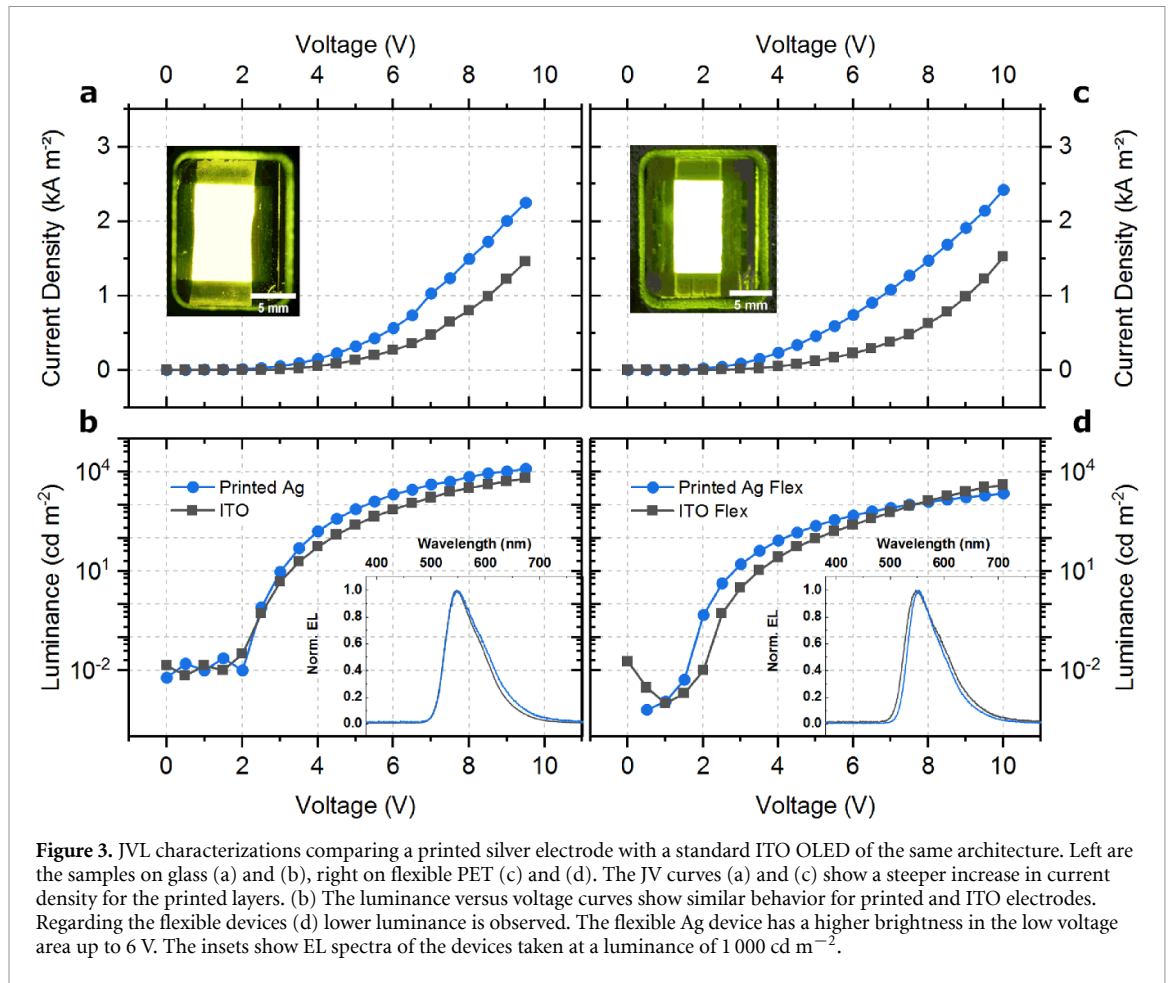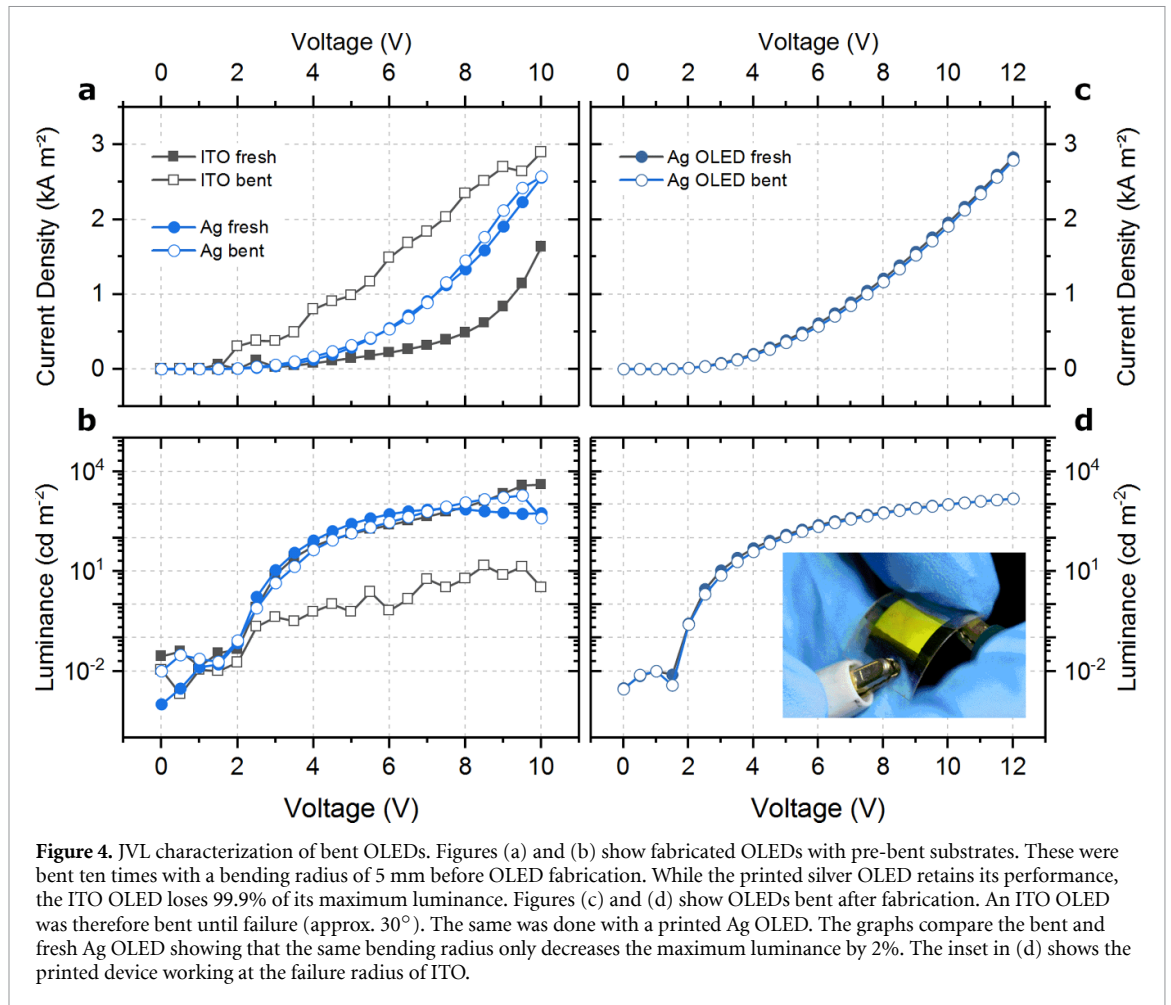
Figure 3. JVL characterizations comparing a printed silver electrode with a standard ITO OLED of the same architecture. Left are the samples on glass (a) and (b), right on flexible PET (c) and (d). The JV curves (a) and (c) show a steeper increase in current density for the printed layers. (b) The luminance versus voltage curves show similar behavior for printed and ITO electrodes. Regarding the flexible devices (d) lower luminance is observed. The flexible Ag device has a higher brightness in the low voltage area up to 6 V. The insets show EL spectra of the devices taken at a luminance of 1 000 cd m^{-2}.

Table 1. Turn-on voltage (V_{on}), luminance (L), current efficacy (η_C) and CIE1931 coordinates of the fabricated OLEDs.

| Electrode | V_{on} (V) | Peak L (cd m^{-2}) | η_C (cd A^{-1}) @ L (cd m^{-2}) | | | Peak η_C (cd A^{-1}) | CIE1931 | |
			100	1000	10 000		x	y
ITO	2.5	16 636	0.78	3.00	4.43	4.54	0.41	0.55
Silver	2.5	11 983	1.26	2.63	5.13	5.34	0.42	0.53
Flex ITO	3.0	3890	0.52	1.92	—	2.71	0.42	0.53
Flex Ag	2.5	2170	0.43	0.79	—	0.89	0.43	0.55

Figures 3(a) and (c) compare the JV characteristics of the device with the printed and the ITO electrodes. While similar current densities are observed at first, the printed electrode quickly surpasses the ITO. For the glass devices the same trend can be observed regarding the luminance/voltage curves shown in figure 3(b). A similar start with comparable turn-on voltages (defined as the voltage where the luminance first surpasses 1 cd m^{-2}) at $V_{on} = 2.5$ V for both electrodes is visible, indicating our printed Ag electrode does not lead to any additional electronic barriers to charge injection in comparison to ITO. Afterwards the luminance of the printed Ag-based OLED exceeds the reference device (in the measured voltage range) as seen in figure 3(b). However, at high voltages, the ITO-based device reaches a higher absolute luminance as can be seen in table 1.

Flexible devices show a similar trend as seen in figure 3(d). Although the electrode itself has a lower transmission, we achieve higher luminance values, which makes the electrode more effective. If the functionality of both electrodes were the same, the lower transmission would negatively affect device performance. However, since we have a higher conductivity, we can achieve an enhanced charge carrier injection into the emission layer, and thus a stronger recombination from it, leading to a higher light output. EL spectra measured at 1000 cd m^{-2} are the same for both devices, as shown in the insets, both show a broad peak with a maximum at 547 nm. Thanks to the uniform transmission over the whole visible spectrum, no color shift in emission is observed for the devices with printed electrodes.

Figure 4. JVL characterization of bent OLEDs. Figures (a) and (b) show fabricated OLEDs with pre-bent substrates. These were bent ten times with a bending radius of 5 mm before OLED fabrication. While the printed silver OLED retains its performance, the ITO OLED loses 99.9% of its maximum luminance. Figures (c) and (d) show OLEDs bent after fabrication. An ITO OLED was therefore bent until failure (approx. 30°). The same was done with a printed Ag OLED. The graphs compare the bent and fresh Ag OLED showing that the same bending radius only decreases the maximum luminance by 2%. The inset in (d) shows the printed device working at the failure radius of ITO.

To determine the current used to produce a certain luminance, the current efficacy η_C can be calculated. This is done by dividing the luminance L (in cd m^{-2}) by the current density j (in A m^{-2}) resulting in the current efficacy (in cd A^{-1}, $\eta_C = L\,j^{-1}$). It was found that after a similar initial efficacy for both the ITO and Ag device, a higher current efficacy is achieved with the printed electrode. The influence of the higher current density is balanced out by the even higher luminance, which results in higher efficacies of the silver devices. This is attributed to the better conductivity of the printed layer compared to the reference ITO. In the case of flexible devices, the overall lower current efficacy is most likely caused by the higher roughness of the PET in comparison to glass. In combination with the crystallinity of the printed silver this can lead to more shorts in the device, lowering the efficacy.

Again, the behavior of the faster growing current density curve can be attributed to the lower sheet resistance of the printed Ag ($R_{sh} = 16\ \Omega$ sq^{-1}) compared to that of ITO ($R_{sh} = 20\ \Omega$ sq^{-1}). While the ITO OLED shows a steeper increase in current efficacy, reaching its maximum of 4.3 cd A^{-1} at a luminance of 6300 cd m^{-2}, the Ag OLED reaches up to 5.3 cd A^{-1} at a luminance of 12 000 cd m^{-2}. The EL spectra of both

device types show a broad peak with a maximum at around 550 nm, corresponding to CIE1931 coordinates of $x = 0.41$ and $y = 0.55$ for the printed Ag-based device, and $x = 0.42$ and $y = 0.53$ for the ITO-based device. The same applies to the flexible OLEDs with CIE1931 coordinates of $x = 0.43$ and $y = 0.55$ for the Ag-OLED, and $x = 0.42$ and $y = 0.53$ for the ITO device.

To verify the possible application in flexible electronics, bending tests were performed. Since bending failure of devices is mostly attributed to the cracking of the ITO during bending [21], OLEDs were fabricated following a pre-bending (ten cycles with 2% cyclic strain) of the flexible ITO and the printed electrodes. Figures 4(a) and (b) show the J–V–L characteristics where it can be seen that the bent ITO OLEDs lose 99% of their maximum luminance while the printed ones show next to no degradation. In a second step, a finished ITO OLED was bent until total failure. Printed silver OLEDs were subsequently bent to the same angle (approx. 30°, see inset in figure 4(d)) and the device characteristics were measured afterwards. Only a small loss in maximum luminance of 2% was observed, making these type of printed OLEDs suitable for potential flex-to-install applications.

4. Conclusion

In conclusion, we have produced printed silver electrodes from a particle-free ink via a low temperature process. The printed layers were analyzed and have shown both, good optical transmission >75% over the whole visible spectrum as well as the required electrical conductivity. For the first time, OLEDs were fabricated incorporating these electrode layers and were shown to be able to surpass ITO-based reference devices with luminances of up to 12 000 cd m^{-2}. Additionally, the printed transparent silver layers showed a high degree of flexibility in comparison to ITO, whose resistance increased severely after only a few bending cycles. With flexible devices, a comparable luminance was achieved for ITO and Ag devices. Bending of the OLEDs was used to demonstrate the superior performance of the printed devices for flex-to-install applications compared to the ones based on ITO.

Acknowledgments

ORCID iDs

Michael Hengge ⬤ https://orcid.org/0000-0003-2488-5870
Konstantin Livanov ⬤ https://orcid.org/0000-0001-6635-5697
Natalia Zamoshchik ⬤ https://orcid.org/0000-0002-9192-8300
Felix Hermerschmidt ⬤ https://orcid.org/0000-0001-8292-4124
Emil J W List-Kratochvil ⬤ https://orcid.org/0000-0001-9206-800X

References

[1] Kim H, Gilmore C M, Piqué A, Horwitz J S, Mattoussi H, Murata H, Kafafi Z H and Chrisey D B 1999 Electrical, optical, and structural properties of indium-tin-oxide thin films for organic light-emitting devices *J. Appl. Phys.* **86** 6451–61

[2] Chopra K L, Major S and Pandya D K 1983 Transparent conductors—a status review *Thin Solid Films* **102** 1–46

[3] Luo M, Liu Y, Huang W, Qiao W, Zhou Y, Ye Y and Chen L S 2017 Towards flexible transparent electrodes based on carbon and metallic materials *Micromachines* **8** 1–16

[4] Peng C, Jia Z, Neilson H, Li T and Lou J 2013 *In situ* electro-mechanical experiments and mechanics modeling of fracture in indium tin oxide-based multilayer electrodes *Adv. Eng. Mater.* **15** 250–6

[5] Semaltianos N G 2001 Thermally evaporated aluminium thin films *Appl. Surf. Sci.* **183** 223–9

[6] Cho H, Yun C and Yoo S 2010 Multilayer transparent electrode for organic light-emitting diodes: tuning its optical characteristics *Opt. Express* **18** 3404

[7] Wu W 2017 Inorganic nanomaterials for printed electronics: a review *Nanoscale* **9** 7342–72

[8] Li D, Lai W-Y, Zhang Y-Z and Huang W 2018 Printable transparent conductive films for flexible electronics *Adv. Mater.* **30** 1704738

[9] Kamyshny A and Magdassi S 2014 Conductive nanomaterials for printed electronics *Small* **10** 3515–35

[10] Hermerschmidt F, Choulis S A and List-Kratochvil E J W 2019 Implementing inkjet-printed transparent conductive electrodes in solution-processed organic electronics *Adv. Mater. Technol.* **4** 1800474

[11] Yang W, List-Kratochvil E J W and Wang C 2019 Metal particle-free inks for printed flexible electronics *J. Mater. Chem.* C **7** 15098–117

[12] Vaseem M, Lee S-K, Kim J-G and Hahn Y-B 2016 Silver-ethanolamine-formate complex based transparent and stable ink: electrical assessment with microwave plasma vs thermal sintering *Chem. Eng. J.* **306** 796–805

[13] Choi Y, Seong K and Piao Y 2019 Metal−organic decomposition ink for printed electronics *Adv. Mater. Interfaces* **6** 1901002

[14] Azulai D, Belenkova T, Gilon H, Barkay Z and Markovich G 2009 Transparent metal nanowire thin films prepared in mesostructured templates *Nano Lett.* **9** 4246–9

[15] Kinner L, List-Kratochvil E J W and Dimopoulos T 2020 Gentle plasma process for embedded silver-nanowire flexible transparent electrodes on temperature-sensitive polymer substrates *Nanotechnology* **31** 365303

[16] Rathmell A R, Bergin S M, Hua Y L, Li Z Y and Wiley B J 2010 The growth mechanism of copper nanowires and their properties in flexible, transparent conducting films *Adv. Mater.* **22** 3558–63

[17] Finn D J, Lotya M and Coleman J N 2015 Inkjet printing of silver nanowire networks *ACS Appl. Mater. Interfaces* **7** 9254–61

[18] Hofmann A I, Cloutet E and Hadziioannou G 2018 Materials for transparent electrodes: from metal oxides to organic alternatives *Adv. Electron. Mater.* **4** 1700412

[19] Hermerschmidt F, Burgués-Ceballos I, Savva A, Sepos E D, Lange A, Boeffel C, Nau S, List-Kratochvil E J W and Choulis S A 2016 High performance indium tin oxide-free solution-processed organic light emitting diodes based on inkjet-printed fine silver grid lines *Flex. Print. Electron.* **1** 035004

[20] Pozov S M *et al* 2019 Up-scalable ITO-free organic light emitting diodes based on embedded inkjet-printed copper grids *Flex. Print. Electron.* **4** 025004

[21] Cho H, Yun C, Park J-W and Yoo S 2009 Highly flexible organic light-emitting diodes based on ZnS/Ag/WO3 multilayer transparent electrodes *Org. Electron.* **10** 1163–9

[22] Hermerschmidt F, Burmeister D, Ligorio G, Pozov S M, Ward R, Choulis S A and List-Kratochvil E J W 2018 Truly low temperature sintering of printed copper ink using formic acid *Adv. Mater. Technol.* **3** 1–6

[23] Greer J R and Street R A 2007 Thermal cure effects on electrical performance of nanoparticle silver inks *Acta Mater.* **55** 6345–9

[24] Niittynen J, Sowade E, Kang H, Baumann R R and Mäntysalo M 2015 Comparison of laser and intense pulsed light sintering (IPL) for inkjet-printed copper nanoparticle layers *Sci. Rep.* **5** 8832

[25] Allen M L, Aronniemi M, Mattila T, Alastalo A, Ojanperä K, Suhonen M and Seppä H 2008 Electrical sintering of nanoparticle structures *Nanotechnology* **19** 175201

[26] Reinhold I, Hendriks C E, Eckardt R, Kranenburg J M, Perelaer J, Baumann R R and Schubert U S 2009 Argon plasma sintering of inkjet printed silver tracks on polymer substrates *J. Mater. Chem.* **19** 3384–8

[27] Wolf F M, Perelaer J, Stumpf S, Bollen D, Kriebel F and Schubert U S 2013 Rapid low-pressure plasma sintering of inkjet-printed silver nanoparticles for RFID antennas *J. Mater. Res.* **28** 1254–61

[28] Wünscher S, Stumpf S, Perelaer J and Schubert U S 2014 Towards single-pass plasma sintering: temperature influence of atmospheric pressure plasma sintering of silver nanoparticle ink *J. Mater. Chem.* C **2** 1642

[29] Knapp C E, Chemin J-B, Douglas S P, Ondo D A, Guillot J, Choquet P and Boscher N D 2018 Room-temperature plasma-assisted inkjet printing of highly conductive silver on paper *Adv. Mater. Technol.* **3** 1700326

[30] David S, Sefiane K and Tadrist L 2007 Experimental investigation of the effect of thermal properties of the substrate in the wetting and evaporation of sessile drops *Colloids Surf.* A **298** 108–14

[31] Chen D and Zachmann H G 1991 Glass transition temperature of copolyesters of PET, PEN and PHB as determined by dynamic mechanical analysis *Polymer* **32** 1612–21

[32] Demirel B, Yaraş A and Elçiçek H 2011 Crystallization behavior of PET materials *BAÜ Fen Bil. Enst. Dergisi Cilt* **13** 26–35 (http://hdl.handle.net/11772/1592)

[33] Wünscher S, Abbel R, Perelaer J and Schubert U S 2014 Progress of alternative sintering approaches of inkjet-printed metal inks and their application for manufacturing of flexible electronic devices *J. Mater. Chem.* C **2** 10232–61

[34] Bromberg V, Ma S, Egitto F D and Singler T J 2013 Highly conductive lines by plasma-induced conversion of inkjet-printed silver nitrate traces *J. Mater. Chem.* C **1** 6842

[35] Gubkin J 1887 Electrolytische metallabscheidung an der freien Oberfläche einer Salzlösung *Ann. Phys., Lpz.* **268** 114–5

[36] Genish I, Irzh A, Gedanken A, Anderson A, Zaban A and Klein L 2010 Coating dielectric substrates by plasma-reduction of metallic ions in solvents *Surf. Coat. Technol.* **204** 1347–52

[37] Ghosh S, Yang R, Kaumeyer M, Zorman C A, Rowan S J, Feng P X L and Sankaran R M 2014 Fabrication of electrically conductive metal patterns at the surface of polymer films by microplasma-based direct writing *ACS Appl. Mater. Interfaces* **6** 3099–104

[38] Dou S, Tao L, Wang R, El Hankari S, Chen R and Wang S 2018 Plasma-assisted synthesis and surface modification of electrode materials for renewable energy *Adv. Mater.* **30** 1–24

[39] Zamoshchik N, Livanov K and Sheynin Y 2020 Method for metal layer formation US2020017974A1

[40] Yildirim O E, Xu Q and Basaran O A 2005 Analysis of the drop weight method *Phys. Fluids* **17** 062107

[41] Harkins W D 1926 The drop-weight method for the determination of surface tension and the weight of the ideal drop *Nature* **117** 690–1

[42] Zhou Y *et al* 2012 A universal method to produce low-work function electrodes for organic electronics *Science* **336** 327–32

[43] Zheng J, Sun B, Yang R, Song X, Li X and Pu Y 2008 Metal Al produced by H$_2$ plasma reduction of AlCl$_3$: a thermodynamic and kinetic study on the plasma chemistry *J. Phys. Chem.* B **112** 12748–52

[44] Kim S-S, Lee H, Na B-K and Song H K 2004 Plasma-assisted reduction of supported metal catalyst using atmospheric dielectric-barrier discharge *Catal. Today* **89** 193–200

[45] The RRUFF Project 2020 Silver R070416 RRUFF (available at: https://rruff.info/Silver/R070416) (Accessed 15 May 2020)

[46] Mampallil D and Eral H B 2018 A review on suppression and utilization of the coffee-ring effect *Adv. Colloid Interface Sci.* **252** 38–54

[47] Glushko O, Klug A, List-Kratochvil E J W and Cordill M J 2017 Monotonic and cyclic mechanical reliability of metallization lines on polymer substrates *J. Mater. Res.* **32** 1760–9

[48] Cordill M J, Glushko O, Kreith J, Marx V M and Kirchlechner C 2015 Measuring electro-mechanical properties of thin films on polymer substrates *Microelectron. Eng.* **137** 96–100

[49] Cordill M J, Glushko O and Putz B 2016 Electro-mechanical testing of conductive materials used in flexible electronics *Frontiers Mater.* **3** 1–11